



Redundancy and Derating Strategies for Modular Multilevel Converter for an Electric Drive

A. F. Cupertino, J. V. M. Farias, H. A. Pereira, P.R. M. Junior, M.M. Stopa and J.T.Resende

Published in:

Journal of Control, Automation and Electrical Systems

DOI (*link to publication from Publisher*):

[10.1007%2Fs40313-019-00537-z](https://doi.org/10.1007%2Fs40313-019-00537-z)

Publication year:

2019

Document Version:

Accepted author manuscript, peer reviewed version

Citation for published version:

A. F. Cupertino, J. V. M. Farias, H. A. Pereira, P. R. M. Junior, M.M. Stopa and J.T. Resende, "Redundancy and Derating Strategies for Modular Multilevel Converter for an Electric Drive," in *Journal of Control, Automation and Electrical Systems*, pp. 1-11, October 2019. doi: 10.1007%Fs40313-019-00537-z

General rights

Copyright and moral rights for the publications made accessible in the public portal are retained by the authors and/or other copyright owners and it is a condition of accessing publications that users recognise and abide by the legal requirements associated with these rights.

- Users may download and print one copy of any publication from the public portal for the purpose of private study or research.
- You may not further distribute the material or use it for any profit-making activity or commercial gain
- You may freely distribute the URL identifying the publication in the public portal

Take down policy

If you believe that this document breaches copyright please contact us at gesepufv@gmail.com providing details, and we will remove access to the work immediately and investigate your claim.

Redundancy and Derating Strategies for Modular Multilevel Converter for an Electric Drive

Paulo Roberto Matias Júnior · João Victor Matos Farias · Allan Fagner Cupertino ·
Heverton Augusto Pereira · Marcelo Martins Stopa · José Tarcísio de Resende

Received: date / Accepted: date

Abstract Reliability is an important issue in medium-voltage (MV) electrical drives. The modular multilevel converter (MMC) is an inherently fault-tolerant topology and an interesting solution when quadratic loads are used. Redundancy strategies can be used to extend system failure capability. The strategies presented in the literature affect the dynamic performance and the power losses of the MMC. In addition, for isolated and inaccessible areas, such as ore slurry pumps, which are widely used in mining industries, the maintenance time and cost are high. This paper compares four redundancy strategies applied in a MMC for an electric drive and presents a derating strategy to maintain the system operating after a greater number of failures. The results showed that hot redundancy

schemes have less impact on the dynamic performance of the system than the strategy that operates with the nominal submodule (SM) number. Besides, hot redundancy presents up to 14.72% more power losses. For quadratic loads, such as the ore slurry pump, it was concluded that, for 14% of failures, the speed reference should be reduced to at least 28% in order to keep the system operating.

Keywords Modular multilevel converter · Electric drives · Redundancy · Derating.

1 Introduction

The 2-level converter is widely used for low-voltage drives due to its robustness and simplicity when operating at this voltage level. The topologies Neutral-Point Clamped (NPC), Active Neutral-Point Clamped (ANPC) and Flying-Capacitor (FLC) are interesting solutions for medium-voltage (MV) solutions up to 6.6 kV (Kouro et al, 2012). The main solutions for motor voltages equal or higher than 6.6 kV are based on cascade converters, such as the converter developed by Robicon Corporation (Hammond et al, 1997; Wakamura et al, 2015). One disadvantage of this system is the need for a zig-zag transformer, which increases the losses, volume and weight of the equipment.

In recent decades, the Modular Multilevel Converters (MMCs) have proven to be a family of high performance and high efficiency converters (Kumar et al, 2018). They are mainly applied in the field of high power, such as High Voltage Direct Current transmission systems (HVDC), Static Synchronous Compensator (STATCOM) and medium-voltage adjustable speed drive systems. MMC has also been studied for energy storage and renewable energy systems (Akagi et al, 2017).

P. R. M. Júnior · J. V. M. Farias
Graduate Program in Electrical Engineering, Federal Center for Technological Education of Minas Gerais, Belo Horizonte, MG, 30421-169 Brazil.
Tel.: +55-33-99949-5518, +55-31-99411-744
E-mail: paulomatiaspq@gmail.com, joaofariasgv.jvmf@gmail.com

A. F. Cupertino
Department of Materials Engineering, Federal Center for Technological Education of Minas Gerais, Belo Horizonte, MG, 30421-169 Brazil.
Tel.: +55-31-3319-7152
E-mail: afcupertino@ieee.org

H. A. Pereira · J.T. Resende
Department of Electrical Engineering, Universidade Federal de Viçosa, Viçosa, MG, 36570-900 Brazil.
Tel.: +55-31-3899-3266
+55-31-3899-6407
E-mail: heverton.pereira@ufv.br, resende@ufv.br

M. M. Stopa
Department of Electrical Engineering, Federal Center for Technological Education of Minas Gerais, Belo Horizonte, MG, 30421-169 Brazil.
Tel.: +55-31-3319-6836
E-mail: marcelo@cefetmg.br

The use of MMC in electric drive systems is very attractive for many reasons, including (Antonopoulos et al, 2014; Hagiwara et al, 2013, 2009):

- Low switching frequency and harmonic content, which reduce the losses and thermal stress in the motor;
- Likely elimination of transformers in line-frequency MV motor drives;
- High-quality output voltages waveforms, which require no additional filtering schemes;
- High performance, since energy costs and environmental awareness are increasing rapidly;
- Inherent fault tolerance.

The Double-Star Half Bridge (DSHB) is the most used MMC topology and is widely employed in HVDC systems (Farias et al, 2018). However, this topology has some limitations in electrical drive application during low speed and high torque, due to the high voltage ripple in the capacitors. References (Kumar et al, 2018; Antonopoulos et al, 2014; Hagiwara et al, 2013; Kumar et al, 2017; Li et al, 2017) propose some methodologies to solve these limitations for loads whose torque is a quadratic function of the motor speed (Li et al, 2017; Hagiwara et al, 2010). This type of load is very common in sectors such as oil and gas, pumping, mining and cement industry. For instance, slurry pumps are widely used in the mining industry instead of trucks or railroad, overall ore transportation costs are significantly reduced (Dove et al, 2019). Such kind of load accounts for about 70% of the market for MV drives (Wu et al, 2017). Some companies, such as Benshaw and Siemens, commercialize the DSHB-MMC topology for pumps, compressors and high-power blower drive systems (Akagi et al, 2017).

Regarding MV electrical drive design for mining applications, a fault tolerance capability is an important issue due to the high cost/failure rate and the fact that out-of-service maintenance is expensive. The converter is the most vulnerable link, especially because of the semiconductor devices and capacitors used in its manufacturing. However, due to advances in power electronics, many high reliability products have been developed (Song et al, 2013). MMC is an inherently fault-tolerant topology, which leads to increased system reliability when redundancy strategies are considered (Ahmed et al, 2015).

The literature presents some works related to MMC redundancy. Reference (Farias et al, 2018) studies different techniques of redundancy applied to STATCOM, while reference (Wang et al, 2017) mentions the importance of redundancy, which allows for a maintenance scheduling, without affecting the remaining system. Reference (Liu et al, 2015) focuses on optimizing MMC redundancy control strategy. Reference (Son et al, 2012) shows the design for

a HVDC system with redundant submodule, SM, targeting uninterruptible energy transfer.

Power reduction strategies have proven to be a potential solution to increase system reliability. Reference (Vernica et al, 2018) discusses a smart derating strategy to obtain the optimum power level of the wind power plant with the longest lifetime. In turn, (Achiri et al, 2015) presents a reduction in the inverter output current in order to avoid high temperatures when the flow and efficiency of the cooler system decrease. Reference (Maharjan et al, 2010) developed a fault-tolerant cascade converter with a neutral displacement in order to continue operating during faults. This method, called neutral shift, consists in the injection of a zero sequence voltage and displacement of the neutral so that the line voltages remain constant to obtain improved performance. Finally, (Song et al, 2010) proposes a fault tolerant cascade converter based on STATCOM. When a fault cell is detected, it is removed from the system and the voltage of each cell increases in order to avoid overmodulation. However, it is not always possible to increase the cell voltage due to the specifications of cell components, since, for a cost-effective design, the margin for increasing the voltage in the cell is reduced or nonexistent.

Regarding the application in electrical drives, it is possible to extend the redundancy study range. Instead of grid connected systems, the electric drive system does not have a minimum operating voltage. Thus, if a larger number of failures occur, the system can still operate at derating mode until maintenance can be programmed and performed. For a slurry pump system located in isolated or inaccessible areas, if more failures occur in the MMC, the derating strategy will keep the slurry pump running, with reduced flow. However, there is a lack of derating strategies for MMC for an electric drive in the literature.

Therefore, this work intends to fulfill this gap with a MMC for an electric drive system. A 1.4 MW slurry pump is used as a mechanical load. This study offers the following contributions:

- Analysis of the redundancy strategies in a DSHB-MMC based medium-voltage electric drive;
- Comparison of the redundancy strategies in terms of power losses and dynamic response;
- Derating strategy design for continuous operation in the event of a large number of failures.

The paper is outlined as follows. Section 2 proposes the MMC drive system and presents the control strategies. The fault-tolerant operation with redundant SMs and derating strategy are presented in Section 3. Section 4 presents the case study and the parameters of the simulated system. Furthermore, the obtained results are shown and discussed

fluctuation of the capacitors at low speed. The CMI is employed at the 0 to 20 Hz range of the motor frequency, where it cause the greatest impact on the voltage ripple. The frequency used is 54 Hz for CMI, and the amplitude of the third harmonic inserted is 1/6 of the fundamental component (Hagiwara et al, 2013).

The individual balancing control is used to ensure that the individual capacitor voltage is balanced according to the reference value (Meynard et al, 2002). For such, the individual controller is composed of a proportional controller, as shown in Fig. 2 (b). The moving average filter (MAF) attenuates the capacitor voltage ripple, which improves the individual balancing performance. Then, its output is multiplied by the arm current, $i_{sm,i}$. The obtained signal is added to the modulator reference signal.

The last control structure is the motor speed control, Fig.2 (c). The rotor field orientation control (RFOC) strategy is used based on (Novotny et al, 1996). The motor position is measured to obtain the necessary motor flux alignment.

The modulator adds, normalizes and compares the reference signal with the carrier waves (Hagiwara et al, 2013, 2009, 2010; Sahoo et al, 2018). A Phase-Shifted PWM (PSPWM) with third harmonic injection is the modulation strategy employed. The normalized reference signals per phase are given by:

$$v_u^* = v_b^* + \frac{v_z^*}{v_{sm,u}^*} - \frac{v_s^*}{v_{sm,u}^* N_{o(u)}} + \frac{v_{com}^*}{v_{sm,u}^* N_{o(u)}} + \frac{1}{2} \frac{N}{N_{o(u,l)}}, \quad (4)$$

$$v_l^* = v_b^* + \frac{v_z^*}{v_{sm,l}^*} + \frac{v_s^*}{v_{sm,l}^* N_{o(l)}} + \frac{v_{com}^*}{v_{sm,l}^* N_{o(l)}} + \frac{1}{2} \frac{N}{N_{o(u,l)}}, \quad (5)$$

where v_b^* is the reference of the individual balancing control, v_z^* is the voltage generated by the control of the circulating current, v_s^* is the reference voltage of the RFOC, $v_{sm,u}^*$ and $v_{sm,l}^*$ are the reference voltages of the SMs of the upper and lower arm, respectively. On the other hand, v_{com}^* is the common mode voltage and $N_{o(u,l)} = \min(N_{o(u)}, N_{o(l)})$.

3 MMC Fault-Tolerant Operation

3.1 Redundancy analysis

Due to several electrical, mechanical and environmental factors present in an industry, MMC is vulnerable to some types of failures or faults (Son et al, 2012). Nevertheless, the system should continue operating perfectly until maintenance can be programmed (Konstantinou et al, 2012). The MMC topology is often featured with its robustness for SM failures. Redundant SMs are inserted into each arm for fault-tolerant operation. When a fault is detected, the damaged SM should be bypassed (Son et al, 2012).

According to (Farias et al, 2018), the redundancy strategies can be classified as: Redundant operation based on Spare SMs (RSS), Redundant operation based on Additional SMs (RAS), Optimized Redundant operation based on

Additional SMs (RASO) and Standard Redundant operation (SR).

The RSS strategy is a redundancy technique based on the concept of spare SMs (Son et al, 2012). During normal operations, the backup SM are bypassed. When a fault is detected, this faulty SM is replaced by the backup SMs (Li et al, 2015). This technique has the advantage of operating with a constant number of SM and requiring no control adaptation. However, this technique affects the transient of all control variables, due the SM capacitor charging process.

The RAS strategy consists in operating the MMC with more SMs than the nominal number. When a fault occurs, the faulty SM is bypassed and the operating voltage of the SMs is maintained at the rated voltage (Saad et al, 2015; Choi et al, 2016). Therefore, when a SM fails, the SMs voltages do not increase. Thus, small transients are observed in the converter dynamics.

On the other hand, RASO strategy operates the SMs with a reduced voltage under normal conditions, thus reducing the voltage stresses and power losses in the SM power devices (Ahmed et al, 2015). When a fault is detected, the SM voltages are increased to avoid overmodulation (Farias et al, 2018).

Finally, the SR strategy operating principle is similar to that of RASO. However, there is no additional SMs. In this technique, when a failure occurs, the operating voltage of the SMs is increased (Liu et al, 2015). This is an interesting solution for applications with high numbers of SMs, which does not require redundant SMs. The utilization factor f_u can be computed by:

$$f_u = \frac{v_{sm}^*}{v_{rated}}, \quad (6)$$

where v_{rated} is the rated voltage of the semiconductor devices. However, to maintain a safe operation, f_u can not exceed 0.6 (Farias et al, 2018). Therefore, this strategy is limited by the maximum voltage stresses at the semiconductor devices and capacitors. According to (Farias et al, 2018), for the SR strategy, the redundancy factor f_r is computed by:

$$f_r = 1 - \frac{f_{u,o}}{f_{u,f}}, \quad (7)$$

where $f_{u,o}$ is the utilization factor under normal conditions, and $f_{u,f}$ is the utilization factor when all admissible failures occur. Many papers in the specialized literature employ f_r around 10% (Konstantinou et al, 2012). The number of redundant SM, M , can be computed by:

$$M = \text{ceil}(N f_r) \quad (8)$$

Manipulation of (7) and (8), results in:

$$k_u = \frac{f_{u,f}}{f_{u,o}} = \frac{N}{N - \text{ceil}(N f_r)}, \quad (9)$$

where k_u indicates the perceptual variation in the utilization factor. Since $f_{u,o} = 0.5$ is widely used, $k_u = 0.6/0.5 = 1.2$ would be the limit. However, once the capacitor voltages of the SMs present ripple, a safety margin is adopted. Thus, $k_u = 1.15$ is employed in this paper. Fig. 3 shows the effect of the number of SMs on the k_u ratio. As observed, applications with fewer number of SMs exceed the range of $k_u = 1.15$, which means that $f_r = 10\%$ can not be reached using the SR strategy. Once MMC based drive systems typically employ few SMs, the SR strategy is not suitable, since it results in large voltage stress in the healthy SMs.

Regarding the implementation, the reference values for the average voltage control v_{avg}^* and the balancing control v_{sm}^* depend on the redundancy strategy adopted. For the RSS and RAS strategies, the voltage reference for the individual control is calculated by:

$$v_{sm}^* = \frac{V_{dc}}{N}, \quad (10)$$

where V_{dc} is the dc-link voltage. Even during faults, the average voltage references do not change in the RSS and RAS strategies. Therefore, the average reference voltage per phase is calculated by:

$$v_{avg}^* = \frac{V_{dc}}{N}. \quad (11)$$

However, in the RASO strategy, when a fault is detected, the SMs voltages reference increase. Thus, the voltage reference for all SMs and the average reference voltage for RASO strategies are computed by:

$$v_{sm}^* = \frac{V_{dc}}{N_{o(u,l)}}, \quad (12)$$

$$v_{avg}^* = \frac{V_{dc}}{N_{o(u,l)}}. \quad (13)$$

Table 1 shows the main characteristics of each redundancy strategy described in this paper. In addition, the number of gate signals for these strategies is given by $12N_o$, since the MMC has 6 arms and 2 IGBTs per SM.

3.2 Derating strategy

As previously mentioned, industrial equipment is susceptible to several factors that can lead to failures. After all redundant SMs have been used, failures can

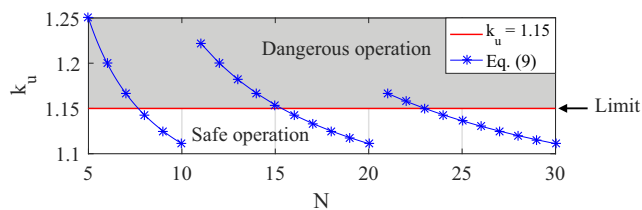


Fig. 3 Redundancy limit for SR for some number of SMs.

Table 1 Main characteristics of redundancy strategies.

Strategy	v_{sm}^*	N_o	M	Ref.
RAS	$\frac{V_{dc}}{N}$	$N + M - F$	$M = \text{ceil}(Nf_r)$	(Saad et al., 2015) (Choi et al., 2016)
RASO	$\frac{V_{dc}}{N_o}$	$N + M - F$	$M = \text{ceil}(Nf_r)$	(Ahmed et al., 2015)
RSS	$\frac{V_{dc}}{N}$	N	$M = \text{ceil}(Nf_r)$	(Son et al., 2012) (Li et al., 2015)
SR	$\frac{V_{dc}}{N_o}$	$N - F$	$M = 0$	(Liu et al., 2015)

still occur. For applications where the electric drive is in inaccessible areas, such as ore slurry pumps in mining industries, the time and cost of maintenance are high. Under such conditions, a derating strategy is proposed in this paper. When the number of failures exceeds the designed redundancy factor, the motor reference speed is reduced to avoid overmodulation. Fig. 4 illustrates this problem. When a fault occurs in a MMC based electric drive without redundant SM, the insertion index is increased, since the MMC will have less SMs available to synthesize the motor voltage. To circumvent this increase in the insertion index and avoid overmodulation, the derating strategy is used to keep the insertion index constant when more failures occur. Thus, the motor voltage is reduced by motor speed reduction. This is possible due to the quadratic characteristic of the load in a certain operating range, since some applications have a shut-off speed.

The voltage of the stator machine in d-q can be represented by (Novotny et al., 1996):

$$v_s = \sqrt{v_{ds}^2 + v_{qs}^2}, \quad (14)$$

where, v_{ds} and v_{qs} are the direct and quadrature stator voltages, respectively.

On the other hand, in a rotor flux reference frame, the steady-state voltages can be described by (Novotny et al., 1996):

$$V_{ds} = R_s I_{ds} - \omega_e L'_s I_{qs}, \quad (15)$$

$$V_{qs} = R_s I_{qs} + \omega_e L_s I_{ds}, \quad (16)$$

where R_s is the stator resistance, I_{ds} and I_{qs} are the steady-state values of the direct and quadrature axis currents, respectively. ω_e is the angular electric frequency of

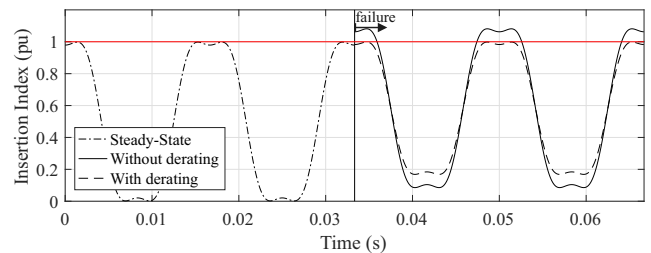


Fig. 4 Effect of derating on the insertion index.

the stator, L'_s is the stator transient inductance, L_s is the stator self inductance. The current I_{qs} can be written according to the torque, as follows:

$$I_{qs} = \frac{4L_r}{3pL_m\lambda_r} T_e, \quad (17)$$

where L_r is the rotor self inductance, p is the number of poles, L_m is the magnetizing inductance and λ_r is the rotor flux. On the other hand, the load torque is given by:

$$T_L = k\omega_m^2, \quad (18)$$

where ω_m is the angular mechanical frequency of the rotor. The constant k is calculated to have the rated torque T_{nom} at nominal speed ω_{nom} . Using relations (15) and (16), and disregarding the friction and $\omega_e \approx \omega_m$, the equation (14) can be written as:

$$v_s = \sqrt{a\omega_m^6 + b\omega_m^4 - c\omega_m^3 + d\omega_m^2 + e^2}, \quad (19)$$

where the constants a , b , c , d and e are respectively:

$$a = \left(\frac{L_r L'_s k}{3pI_{ds} L_m^2} \right)^2, \quad (20)$$

$$b = \left(\frac{R_s L_r k}{3pL_m^2 I_{ds}} \right)^2, \quad (21)$$

$$c = \left(\frac{2R_s L_r L'_s k}{3pL_m^2} \right)^2, \quad (22)$$

$$d = (L_s I_{ds})^2 - \left(\frac{2R_s L_r L'_s k}{3pL_m^2} \right)^2, \quad (23)$$

$$e = (R_s I_{ds})^2. \quad (24)$$

For high speed operation, most of the voltage synthesized by the MMC is due to the RFOC control and the average control, since the voltage generated by the circulating and balancing controls is very low at high speeds. Therefore, the normalized voltages synthesized for the upper and lower arm can be approximated by:

$$v_u \approx -\frac{v_s}{v_{sm,u}^* N_{o(u)}} + \frac{1}{2} \frac{N}{N_{o(u,l)}}, \quad (25)$$

$$v_l \approx \frac{v_s}{v_{sm,l}^* N_{o(l)}} + \frac{1}{2} \frac{N}{N_{o(u,l)}}. \quad (26)$$

Thereby, the maximum values of the synthesized upper and lower arm normalized voltages are given by:

$$\max(v_{u,l}) = \max\left(\frac{v_s}{v_{sm(u,l)}^* N_{o(u,l)}}\right) + \max\left(\frac{1}{2} \frac{N}{N_{o(u,l)}}\right) \leq 1. \quad (27)$$

By assuming a modulation index equal to 1 to avoid overmodulation, the following result is obtained:

$$v_s + v_{sm}^* N_{o(u,l)} \left(\frac{1}{2} \frac{N}{N_{o(u,l)}} - 1 \right) = 0. \quad (28)$$

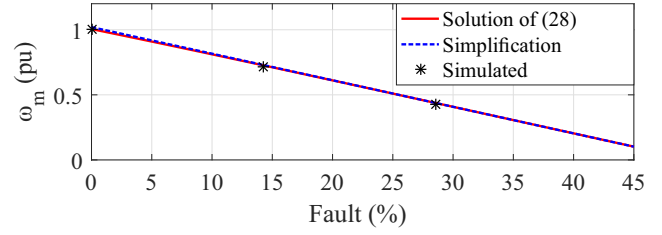


Fig. 5 Speed reduction according to the SM fault percentage.

Thus, replacing (19) in (28), and solving for ω_m , the necessary reduction of the speed can be obtained, according to the number of failures. For the sake of simplicity and processing time, (19) can be simplified due to the system parameters. When the typical values are replaced, the constant d has the greatest impact on (19), which can be rewritten as:

$$v_s \approx \sqrt{d\omega_m^2}. \quad (29)$$

Fig. 5 presents the solution and simplification of (28) using the parameters of Tabs. 2 and 3. Note that despite the nonlinear characteristic of (28), the speed reduction is approximately a straight line function with an angular coefficient $\alpha = -2$, due to some facts: firstly, since the motor is controlled by the RFOC, the operation of the motor at high speeds is similar to a constant V/f ratio, which would imply a proportional reduction. Moreover, as failures occur, the difference between the dc link and the sum of the capacitor voltages increases and an additional voltage portion must be used to limit the circulating current. This portion is represented by the term $\frac{1}{2} \frac{N}{N_{o(u,l)}}$, which reduces the voltage to avoid overmodulation.

4 Case Study

The drive used in the tests carried out in this work consists of a 1.4 MW, 7.2 kV, 1792 rpm induction motor that drives a slurry pump. The motor parameters are reported in Table 2. MMC ratings are shown in Table 3. The MMC has 7 SM per arm, but, according to Fig. (3), the SR redundancy strategy can not be used, since, in this case, k_u is greater than the limit 1.15.

The failure scenario used in this paper consists of an asymmetrical failure. When any SM of one arm fails, the other arms continue operating normally. The simulations are performed in the PLECSTM environment, aiming to compare the redundancy strategies for dynamic behavior and power losses. In addition, the derating strategy proposed in this paper will be evaluated through the dynamic behavior of the converter and motor. The ABB IGBT part number 5SNG 0250P330305 of 3.3 kV-250 A is selected for this application.

Table 2 Parameters of the induction motor.

Parameter	Value
Rated active power (P)	1.4 MW
Rated rms line-to-line voltage (v_m)	7.2 kV
Rated line current (i_s)	134 A
Rated frequency (f)	60 Hz
Rated rotational speed (n_m)	1792 rpm
Rated power factor	0.87
Rated efficiency (η)	96.7%
Number of poles (p)	4
Rated torque (T_{nom})	7.46 kN
Rotor resistance (R_r)	0.15386 Ω
Stator resistance (R_s)	0.13735 Ω
Magnetizing inductance (L_m)	217.3 mH
Stator self inductance (L_s)	224.64 mH
Rotor self inductance (L_r)	224.64 mH
Stator transient inductance (L'_s)	14.44 mH

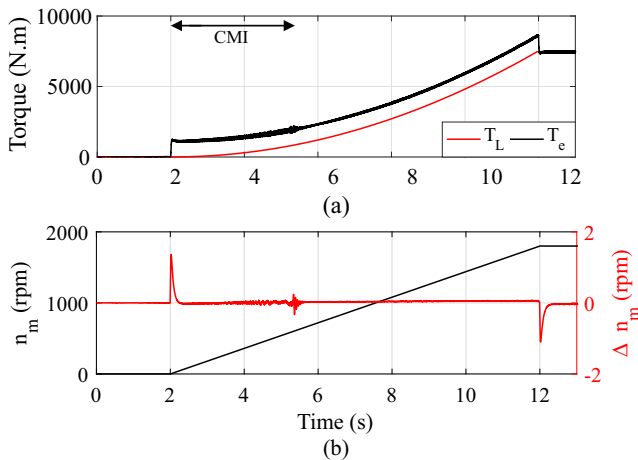
Table 3 MMC ratings.

Parameter	Value
Rated apparent power (S)	2 MVA
Pole to pole dc voltage (V_{dc})	12 kV
Arm inductance (L_{arm})	7.7 mH
Arm resistance (R_{arm})	0.065 Ω
SM capacitance (C)	2 mF
Nominal SM voltage ($v_{sm,n}$)	1.71 kV
Switching frequency (f_s)	945 Hz
Number of SMs (N)	7 per arm
Number of additional/spare SMs (M)	1 per arm

5 Results

5.1 Start-up dynamic performance

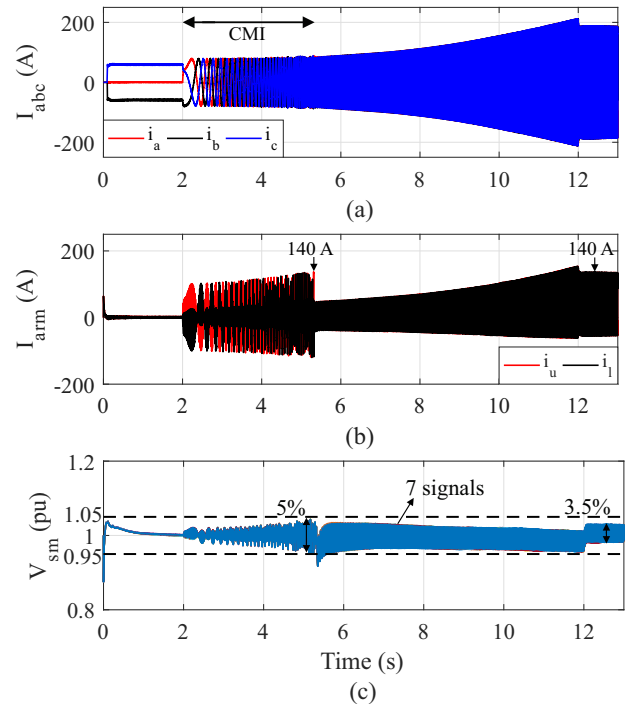
Fig. 6 shows the torque and speed profile applied to the system. Fig. 6 (a) shows the load torque applied to the motor shaft and the electromagnetic torque developed. The difference in the transient is due to the acceleration of the motor, and the developed torque must be higher than the load torque. The oscillations present at $t = 5.3$ s are due to the end of the CMI. There is a very low ripple in the torque,

**Fig. 6** Start-up of the MMC based electric drive: (a) Torque; (b) Mechanical speed and speed error.

which tends to minimize vibrations in the motor, since the converter has 7 SMs and, consequently, 15 levels of phase voltage. The motor speed profile adopted in this paper can be observed in Fig. 6 (b). The motor is accelerated from 2 to 12 seconds, and, in steady-state, the motor speed is maintained at 1800 rpm. In addition, this figure illustrates the speed error during the start-up, which results in a maximum error of 1.5 rpm in $t = 2$ s. The small speed variation in $t = 5.3$ s is caused by the end of the CMI used.

Fig. 7 shows the converter dynamics. Initially, all capacitors of the SMs were considered charged. At 0.1 seconds, the direct axis current was inserted in order to magnetize the motor. This behavior can be analyzed in the motor currents, shown in Fig. 7 (a), when the dc component is applied in the machine. After 2 seconds, a speed ramp was applied to accelerate the motor. At this time, the CMI strategy was inserted to mitigate ripple under lower capacitor voltages frequency. In addition, the same figure shows a quadratic increase in the amplitude of the currents, which is also presented in Fig. 7 (b). When the motor reaches 1800 rpm, a small drop is observed in the stator currents and arm currents.

Moreover, Fig. 7 (b) illustrates the insertion of the i_{zac}^* . This component is injected into the system until $t = 5.3$ s, when the frequency applied to the motor is lower than 20 Hz. It is also demonstrated that the peak of the current inserted in low frequency is similar to the arm currents in steady-state. The SMs capacitor voltages of the upper arm

**Fig. 7** Effect of the start-up in the MMC dynamics: (a) Stator currents; (b) Arm currents; (c) SM voltages.

for the a -phase are shown in Fig. 7 (c). As observed, the capacitor voltages in the steady-state have a ripple of 3.5%, that is, within the 10% dashed band in the figure. During the transient, the ripple reaches a maximum of 10.5%.

5.2 Dynamic Performance of Redundancy Strategies

The simulation considers a failure of one SM at 14 seconds. The capacitor voltages in pu of the upper arm for the a -phase are illustrated in Fig. 8. As observed in Fig. 8 (a), the SM voltages are balanced for the RAS strategy, since the reference voltage of the SMs is maintained constant in this strategy. Additionally, the maximum value of SM voltages in steady-state does not exceed 5%, thus validating the redundancy strategy.

For the RASO strategy, as illustrated in Fig. 8 (b), the SMs operate with reduced voltage under normal conditions, namely 0.9 pu. When failures occur, the SM voltages are increased to avoid overmodulation. The increased reference voltage generates a transient response at the capacitor voltages, which reach the steady-state rapidly, maintaining the voltage at 1 pu. As observed, the capacitor voltages do not exceed the tolerance range of 5%.

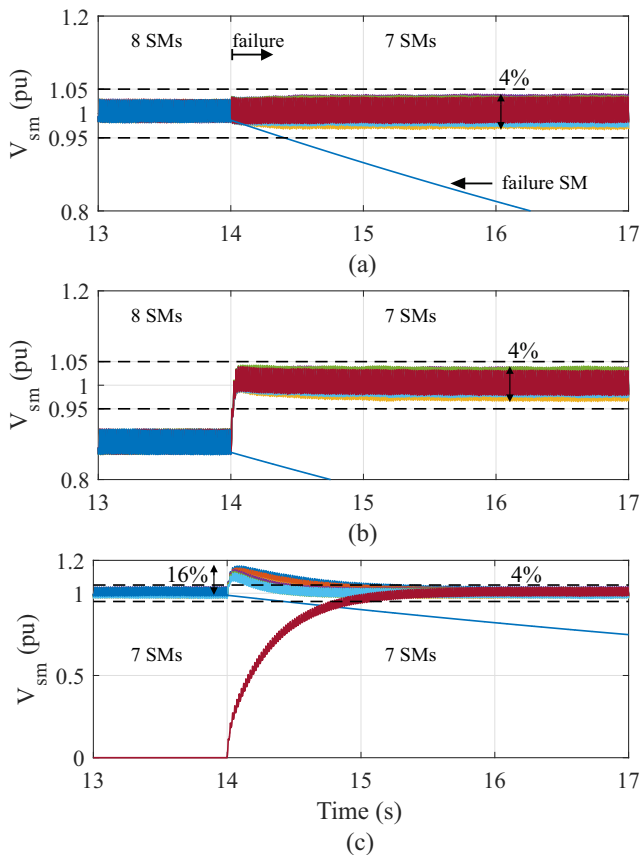


Fig. 8 Effect of the redundancy strategies on the dynamics of the SM voltages: (a) RAS; (b) RASO; (c) RSS.

Fig. 8 (c) illustrates the SMs voltage for the RSS strategy. When the failure occurs, the spare SMs are inserted and their charging process is started due the MMC control. During the charging process, the SM voltages reach 1.16 pu. After 2 s, the spare SM charging process is finished and the converter reaches the steady-state. It is important to observe that the number of SMs does not change in the RSS strategy, since the faulty and spare SMs are exchanged. Although a significant transient is observed during the charge of the spare SM, the voltages have a ripple of less than 5% in steady-state.

The impact of the redundancy strategies on the arm current for the a -phase can be analyzed in Fig. 9. As observed in Fig. 9 (a), no significant transients were observed for the RAS strategy. RASO presents a 21% overshoot, due to the increased voltage reference, as observed in Fig. 9 (b). Finally, Fig. 9 (c) presents the response for RSS. As observed, this strategy presented an 6% overshoot and a total harmonic distortion (THD) of 11.35%. These distortions are consequences of charging the spare SMs, where the individual control imposes a greater proportional action to carry out the charging process.

Fig. 10 shows the electrical and mechanical performance of RFOC. The electromagnetic torque and the speed error for all redundancy strategies are presented in Fig. 10 (a) and Fig. 10 (b), respectively. As observed, when a fault occurs, the RASO strategy presents greater error during the

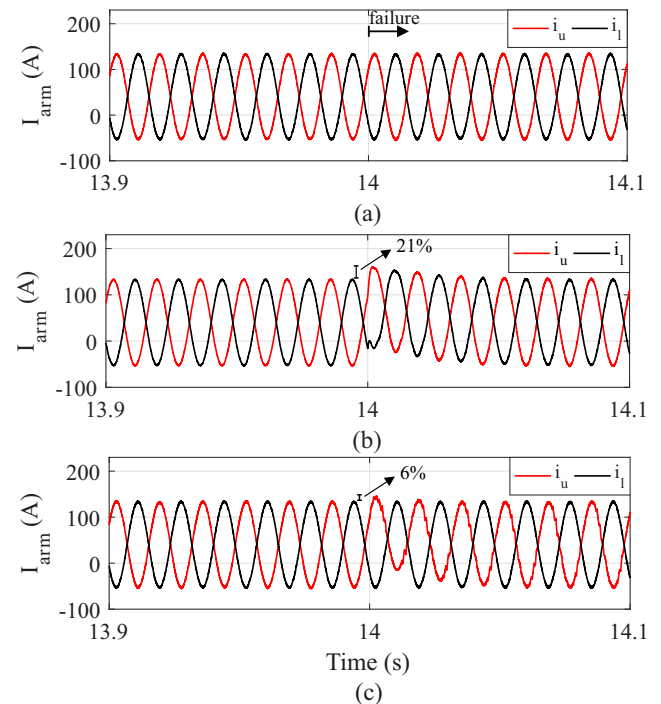


Fig. 9 Effect of the redundancy strategies on the dynamics of the MMC arm currents: (a) RAS; (b) RASO; (c) RSS.

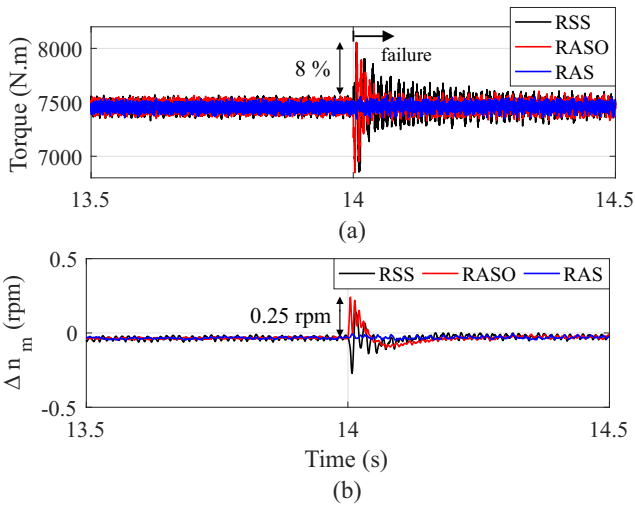


Fig. 10 Effect of the redundancy strategies in the motor dynamics: (a) Torque; (b) Speed error.

transient, but the speed error was only 0.25 rpm, without significantly impacting the RFOC control.

Finally, the conduction and switching power losses of the semiconductors were obtained in steady-state before the failure. The obtained values are represented in Table 4. As observed, the RAS strategy has greater losses in the steady-state, since it works with additional SM. The RASO strategy has slightly lower losses, due to the fact that the semiconductor devices work with reduced voltage before the failure. In turn, the RSS strategy does not affect the efficiency of the system, since MMC operates with the nominal SM number, once the spare SMs are bypassed.

5.3 Dynamic Performance of Derating Strategy

Finally, the derating strategy was implemented. Fig. 11 shows the speed profile to maintain the MMC operating correctly. The first derating occurs at $t = 17$ s, when the second SM failure, and the failure SM is bypassed. As

Table 4 Power losses in the semiconductors devices before the failure.

Strategy	Cond. (W)	Sw. (W)	Increase of losses
RAS	5030	8530	14.72%
RASO	4950	7380	4.31%
RSS	4380	7440	0%

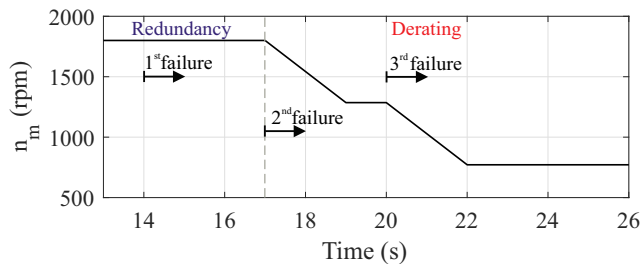


Fig. 11 Reference speed decrease computed by the derating.

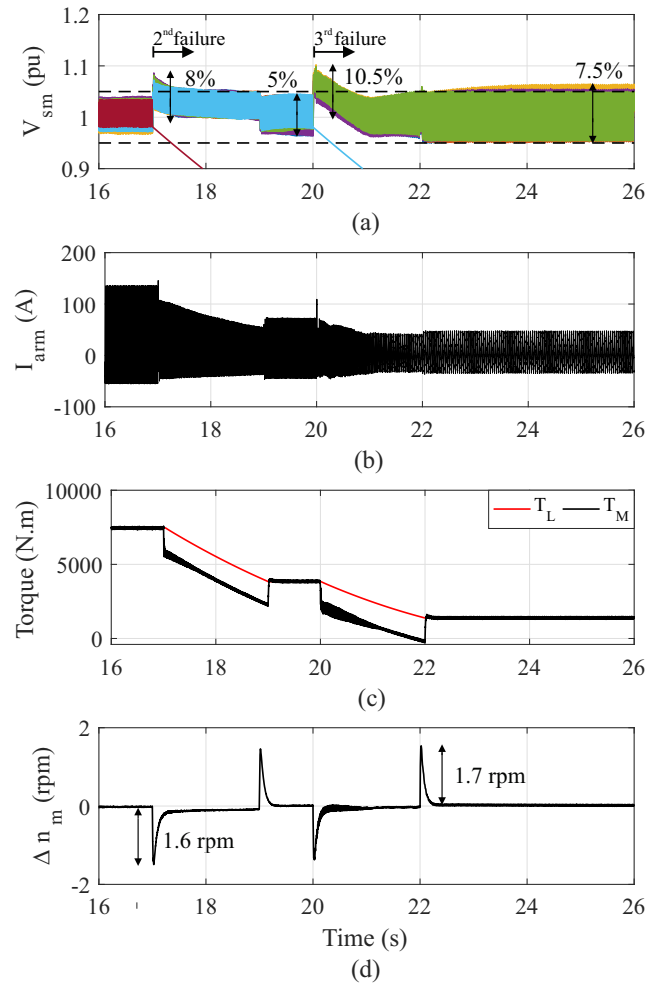


Fig. 12 Derating strategy: (a) SM voltages; (b) Upper arm currents; (c) Torque; (d) Speed error.

already discussed, the speed should be reduced to 28% to maintain the modulation index constant. After reaching the final condition at $t = 19$ s, the motor speed is kept constant to obtain a steady-state condition. Next, the third failure occurs at $t = 20$ s, where the failure SM is bypassed in the converter. The speed is then reduced to 46% of the rated speed, and reaches the final value at 22 seconds.

The MMC and motor dynamics during the derating strategy are shown in Fig. 12. Fig. 12 (a) shows the dynamic behavior of the upper arm capacitor voltages from a -phase. It is observed an overshoot of 1.08 pu at $t = 17$ s due to the second SM failure. In steady-state, at $t = 19$ s, the capacitor voltage is already within the 5% ripple range. In the third fault, at $t = 20$ s, the overshoot is higher, with a peak of 1.105 pu. This can be explained by the low number of SMs operating. However, the ripple in steady-state is 7.5%, which maintains the good functioning.

The upper arm current of a -phase is shown in Fig. 12 (b). During the second failure, at $t = 17$ s, a small overshoot is observed for a short period of time. While the speed is being

reduced, from 17 to 19 seconds, it is possible to analyze the current reduction, due to the load characteristic. For the third fault, a smaller current peak is observed, almost reaching 115 A.

The motor dynamics resulting from the derating strategy can be analyzed in Fig. 12 (c) and (d). The torque applied to the motor, and the developed torque on the shaft are shown in Fig. 12 (c). This figure also shows the torque reduction by the speed reduction strategy used. On the other hand, the speed error is shown in Fig. 12 (d). Despite the considerable transients present in the derating strategy, the speed error is very low. In the second failure, the highest speed error was 1.6 rpm, and in the third, 1.7 rpm. Therefore, it can be concluded that the derating strategy proposed in this paper presented good dynamic results both in MMC and in the motor.

6 Conclusions

This work presented strategies to explore the redundancy capability of the MMC drive system. Four redundancy strategies and a derating strategy were used, whose performances were obtained through a case study of an electric drive of a 1.4 MW slurry pump system. The RAS strategy presents better dynamic behavior, since its voltage reference is maintained fixed. A weakness of this strategy is the highly increased power losses, about 14.72%. The RASO strategy has a significant impact on the MMC dynamics. However, the advantage is allowing semiconductors and capacitors to operate at lower voltages, which increases the power losses by only 4.31%. Finally, the RSS strategy has greater impact on the dynamics due to the capacitor charging process, and presents a 16% overshoot in the voltage of the SMs capacitors at the time of failure. However, the advantages include the fact that only N SMs operate, which does not require the control to be adaptive and that the power losses do not increase. The SR strategy is not suitable for few SMs because it results in large voltage stress in the SMs.

A derating strategy has been proposed, so that MMC can continue to operate when a large number of failures occur. Therefore, for the slurry pump, the speed reference must be reduced by twice the fault percentage, i.e, if there is a 14% faulty SM, the speed reference must be reduced by 28%. However, the derating strategy has an interesting cost/effective solution for emergency situations in isolated mines, since the reduced speed will only imply the ore slurry flow decrease. The derating strategy proposed in this paper was verified through the dynamic behavior of the system and the MMC based electric drive was able to continue operating at derating mode after two extra SM failures.

7 Acknowledgment

This study was financed in part by the Coordenação de Aperfeiçoamento de Pessoal de Nível Superior - Brasil (CAPES) - Finance Code 001, Conselho Nacional de Desenvolvimento Científico e Tecnológico (CNPq) and Fundação de Amparo à Pesquisa do Estado de Minas Gerais (FAPEMIG).

References

- S. Kouro, J. Rodriguez, B. Wu, S. Bernet, M. Perez. (2012). Powering the future of industry: High-power adjustable speed drive topologies, *IEEE Industry Applications Magazine* 18 (4) 26–39.
- P. W. Hammond. (1997). A new approach to enhance power quality for medium voltage ac drives, *IEEE Trans. on Industry Applications* 33 (1) 202–208.
- W. Kawamura, K. L. Chen, M. Hagiwara, H. Akagi. (2015). A low-speed, high-torque motor drive using a modular multilevel cascade converter based on triple-star bridge cells (mmcc-tsbc), *IEEE Trans. on Industry Applications* 51 (5) 3965–3974.
- Y. S. Kumar, G. Poddar. (2018). Medium-voltage vector control induction motor drive at zero frequency using modular multilevel converter, *IEEE Trans. on Industrial Electronics* 65 (1) 125–132.
- H. Akagi. (2017) Multilevel converters: Fundamental circuits and systems, *Proceedings of the IEEE* 105 (11) 2048–2065.
- A. Antonopoulos, L. Ångquist, S. Norrga, K. Ilves, L. Harnefors, H. P. Nee. (2014). Modular multilevel converter ac motor drives with constant torque from zero to nominal speed, *IEEE Trans. on Industry Applications* 50 (3) 1982–1993.
- M. Hagiwara, I. Hasegawa, H. Akagi. (2013). Start-up and low-speed operation of an electric motor driven by a modular multilevel cascade inverter, *IEEE Trans. on Industry Applications* 49 (4) 1556–1565.
- M. Hagiwara, H. Akagi. (2009). Control and experiment of pulsewidth-modulated modular multilevel converters, *IEEE Trans. on Power Electronics* 24 (7) 1737–1746.
- J. V. M. Farias, A. F. Cupertino, H. A. Pereira, S. I. S. Junior, R. Teodorescu. (2018). On the redundancy strategies of modular multilevel converters, *IEEE Trans. on Power Delivery* 33 (2) 851–860.
- Y. S. Kumar, G. Poddar. (2017). Control of medium-voltage ac motor drive for wide speed range using modular multilevel converter, *IEEE Trans. on Ind. Electronics* 64 (4) 2742–2749.
- B. Li, S. Zhou, D. Xu, S. J. Finney, B. W. Williams. (2017). A hybrid modular multilevel converter for medium-voltage variable-speed motor drives, *IEEE Trans. on Power Electronics* 32 (6) 4619–4630.
- M. Hagiwara, K. Nishimura, H. Akagi. (2010). A medium-voltage motor drive with a modular multilevel pwm inverter, *IEEE Trans. on Power Electronics* 25 (7) 1786–1799.
- ‘Pumps and Systems - Slurry Pumps’. (2019). <https://dovemining.com/gravel-pumps/>, accessed 30 May 2019.
- B. Wu, N. Narimani. (2017). *High-Power Converters and AC Drives*, Wiley IEEE Press, 2017.
- Y. Song, B. Wang. (2013). Survey on reliability of power electronic systems, *IEEE Trans. on Power Electronics* 28 (1) 591–604.
- N. Ahmed, L. Ångquist, A. Antonopoulos, L. Harnefors, S. Norrga, H. P. Nee. (2015) Performance of the modular multilevel converter with redundant submodules, in: *IECON 2015 - 41st Annual Conference of the IEEE Industrial Electronics Society*, pp. 003922–003927.
- B. Wang, X. Wang, Z. Bie, P. D. Judge, X. Wang, T. C. Green. (2017). Reliability model of mmc considering periodic preventive maintenance, *IEEE Trans. on Power Delivery* 32 (3) 1535–1544.
- G. Liu, Z. Xu, Y. Xue, G. Tang. (2015). Optimized control strategy based on dynamic redundancy for the modular multilevel converter, *IEEE Trans. on Power Electronics* 30 (1) 339–348.

- G. T. Son, H. J. Lee, T. S. Nam, Y. H. Chung, U. H. Lee, S. T. Baek, K. Hur, J. W. Park. (2012). Design and control of a modular multilevel hvdc converter with redundant power modules for noninterruptible energy transfer, *IEEE Trans. on Power Delivery* 27 (3) 1611–1619.
- I. Vernica, K. Ma, F. Blaabjerg. (2018). Optimal derating strategy of power electronics converter for maximum wind energy production with lifetime information of power devices, *IEEE Journal of Emerging and Selected Topics in Power Electronics* 6 (1) 267–276.
- H. M. N. Achiri, V. Smidl, Z. Peroutka. (2015). Mitigation of electric drivetrain oscillation resulting from abrupt current derating at low coolant flow rate, in: *IECON 2015 - 41st Annual Conference of the IEEE Industrial Electronics Society*, pp. 003638–003642.
- L. Maharjan, T. Yamagishi, H. Akagi, J. Asakura. (2010) Fault-tolerant operation of a battery-energy-storage system based on a multilevel cascade pwm converter with star configuration, *IEEE Transactions on Power Electronics* 25 (9) 2386–2396.
- W. Song, A. Q. Huang. (2010). Fault-tolerant design and control strategy for cascaded h-bridge multilevel converter-based statcom, *IEEE Transactions on Industrial Electronics* 57 (8) 2700–2708.
- B. Gemmel, J. Dorn, D. Retzmann, D. Soerangr. (2008). Prospects of multilevel vsc technologies for power transmission, in: *IEEE/PES Transmission and Distrib. Conf. and Exposition*, pp. 1–16.
- L. Harnefors, A. Antonopoulos, S. Norrga, L. Angquist, H. P. Nee. (2013). Dynamic analysis of modular multilevel converters, *IEEE Trans. on Industrial Electronics* 60 (7) 2526–2537.
- T. A. Meynard, H. Foch, P. Thomas, J. Courault, R. Jakob, M. Nahrstaedt. (2002). Multicell converters: basic concepts and industry applications, *IEEE Trans. on Industrial Electronics* 49 (5) 955–964.
- D. W. Novotny, T. Lipo. (1996). *Vector Control and Dynamics of AC Drives*, Clarendon Press, 1996.
- S. K. Sahoo, T. Bhattacharya. (2018). Phase-shifted carrier-based synchronized sinusoidal pwm techniques for a cascaded h-bridge multilevel inverter, *IEEE Trans. on Power Electronics* 33 (1) 513–524.
- G. S. Konstantinou, M. Ciobotaru, V. G. Agelidis. (2012). Effect of redundant sub-module utilization on modular multilevel converters, in: *IEEE International Conf. on Ind. Technology*, pp. 815–820.
- B. Li, Y. Zhang, R. Yang, R. Xu, D. Xu, W. Wang. (2015). Seamless transition control for modular multilevel converters when inserting a cold-reserve redundant submodule, *IEEE Trans. on Power Electronics* 30 (8) 4052–4057.
- H. Saad, X. Guillaud, J. Mahseredjian, S. Denetière, S. Nguéfeu. (2015). Mmc capacitor voltage decoupling and balancing controls, *IEEE Trans. on Power Delivery* 30 (2) 704–712.
- J. Choi, B. Han, H. Kim. (2016). New scheme of phase-shifted carrier pwm for modular multilevel converter with redundancy submodules, *IEEE Trans. on Power Delivery* 31 (1) 407–409.